Complex phase diagram of $Ce_{0.75}La_{0.25}B_6$ studied by muon spin rotation and relaxation in zero and nonzero external fields

A. Schenck and F. N. Gygax
Institute for Particle Physics of ETH Zürich (IPP), CH-5232 Villigen PSI, Switzerland

G. Solt
Paul Scherrer Institut (PSI), CH-5232 Villigen PSI, Switzerland

(Received 20 September 2006; revised manuscript received 28 November 2006; published 24 January 2007)

The static and dynamic behavior of the local magnetic fields across the phase diagram and at the phase transitions of $Ce_{0.75}La_{0.25}B_6$ was investigated. Different routes in the phase diagram were followed, either by varying the temperature T at constant applied fields $\boldsymbol{B}_{\text{ext}}$ or varying the field at fixed T. It was found that a well-established long-range magnetic order in phase III, characterizing parent CeB_6, is absent here and is replaced by a short-range order (SRO) or more or less random order. This "order" persists in phase IV but, in zero field, with rising temperature in a decreasing volume fraction approaching zero at the IV-I transition. Such "phase separation" is not seen in the presence of an applied field ($\gtrsim$0.3 T). The observed SRO in phase IV is consistent with the mesoscopic SRO dipolar magnetism put forward on the basis of recent resonant x-ray scattering data. On varying T at fixed $\boldsymbol{B}_{\text{ext}}$, both the transitions IV-I and II-III appear as a cusp in the spin-lattice relaxation rate λ. The μ^+ Knight shift appears insensitive to the various phase transitions, in particular to the I-II transition, in sharp contrast to the case in CeB_6.

DOI: 10.1103/PhysRevB.75.024428 PACS number(s): 75.25.+z, 71.27.+a, 76.75.+i, 75.40.Cx

I. INTRODUCTION

Electric and magnetic multipolar interactions between f-shell ions in the solid state and the observation of various types of multipolar ordering have motivated intensive experimental and theoretical research in recent years. The attraction of the field lies in the rich variety of cooperative mechanisms implied by the different possible charge and current distributions in the incomplete f shells, provided the degeneracy of the electronic ground state, left after the crystal field splitting of the ionic multiplet, remains sufficiently large.

Among solids with multipolar ordering, a large body of results are available for the rare earth hexaborides and, in particular, for CeB_6. In this compound the Ce^{3+} ions (ground-state J multiplet $4f^1$, $^2F_{5/2}$) form the corners of a primitive cubic lattice, surrounded by B_6 octahedrons in the cube centers, Fig. 1. The cubic crystal field splits the ionic sextet into a quartet Γ_8 that becomes the ground state[1] and a doublet Γ_7. The doublet level with an excitation energy[2] of $\approx$46 meV can safely be ignored at temperatures $T<10$ K where the multipolar transitions occur, but the remaining orbital and spin degrees of freedom within the quartet Γ_8 alone suffice to form magnetic-dipole and magnetic-octupole as well as electric-quadrupole moments of different symmetries and arbitrary orientations at the Ce^{3+} ions. This means a freedom of not less than 15 possible order parameters and their various combinations.[3]

From the competition and interplay of multipolar interactions a number of various ordered configurations can thus be expected, each corresponding to a certain range of values of the external parameters (temperature, strength and orientation of an applied magnetic field $\boldsymbol{B}_{\text{ext}}$, pressure, uniaxial stress).

The large body of experimental results on CeB_6 (Ref. 2 and 4–19) indeed revealed, beside a high-temperature paramagnetic (PM) phase I, a transition at temperature T_Q to an antiferroquadrupolarly (AFQ) ordered phase II and, on decreasing T, a further transition at $T_N<T_Q$ to a complex, modulated dipolar antiferromagnetic (AFM) phase III,[9] where the AFQ-AFM phase boundary in the T-B plane depends on the direction of $\boldsymbol{B}_{\text{ext}}$.[18] Direct evidence[19] for the AFQ order in CeB_6 was given by the resonant x-ray scattering (RSX) technique, specifically sensitive to the nonsphericity of orientationally ordered scattering ions. The reduced symmetry at the Ce^{3+} sites of the two sublattices forming the AFQ structure splits the Γ_8 levels into pairs of Kramers doublets, and in applied magnetic fields an additional dipolar magnetic structure is induced, coexisting in phase II with AFQ order. A peculiar feature of CeB_6 is the initial increase of T_Q with B along the AFQ-AFM phase boundary: a not too strong magnetic field stabilizes the AFQ order, and only at $B_{\text{ext}}\approx 35$ T (near the theoretical estimate[20]) is the slope of the phase boundary reversed.[7] Present understanding of this behavior is[3] that in the Γ_8 subspace the magnetic field in-

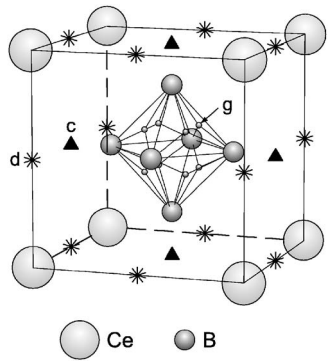

FIG. 1. Crystal structure of cubic CeB_6. The μ^+ are located at the d sites: $(\frac{1}{2}00)$, $(0\frac{1}{2}0)$, and $(00\frac{1}{2})$.

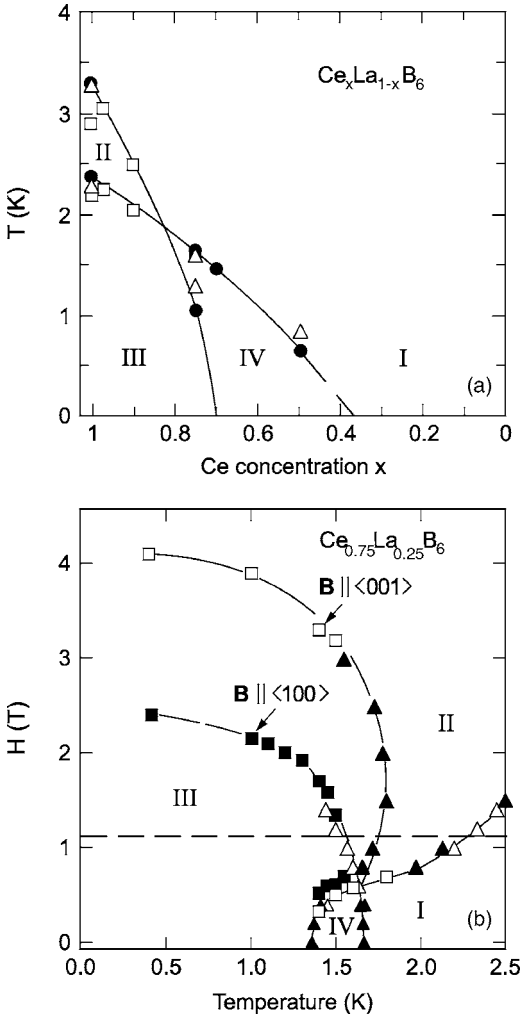

FIG. 2. (a) Phase diagram of $Ce_xLa_{1-x}B_6$ in the temperature–Ce-concentration plane, Refs. 26 and 27; (b) phase diagram of $Ce_{0.75}La_{0.25}B_6$ in the field-temperature plane, Ref. 28.

duces not only dipolar but also magnetic-octupole moments which, at moderately strong fields, strengthen the AFQ order in its competition with the dipolar forces. Octupolar interactions were also invoked to understand the complex magnetic structure of the AFM phase III.[9]

While the basic questions about the phase transitions in CeB_6 seem to be settled now, unexpected phenomena have been observed in the Ce-based ternary rare earth hexaborides $Ce_xR_{1-x}B_6$ (R=La,[21–37] Nd,[38] Pr[22]). Of these, the dramatic change of the phase diagram of CeB_6 due to solute La^{3+} ions is of primary interest. The $Ce_xR_{1-x}B_6$ system, with randomly distributed La ions on the Ce sublattice, is principally the simplest of the $CeRB_6$ ternary alloys. Yet, although the solute ions are "merely" f-shell vacancies on the Ce sublattice, the effect of substitutional La is spectacular: beside the three phases of CeB_6 a new modification with a "hidden" order parameter, phase IV appears. The drastic changes in the phase diagram show how close is the competition between the multipolar interactions that characterize the differently ordered phases. As Fig. 2(a) shows, increasing La content makes both T_Q and T_N decrease, but T_Q faster than T_N, since the "f vacancies" affect the short-ranged quadrupolar ion-ion interactions, prevailing in phase II, more strongly than the dipolar ones dominating in phase III. At the composition $x \approx 0.82$ quadrupolar and dipolar interactions reach a perfect balance, $T_N = T_Q$, but with further increase of the La content obviously a third kind of multipolar interaction becomes dominating, bringing about its own, new order parameter. There is today strong evidence that the hidden order in phase IV is primarily an alignment of octupole moments, coexisting with a short-range-ordered secondary dipolar magnetism. Still, there are as yet several questions open, first of all related to the concomitant presence of the dipolar component, which, curiously, does not seem to disappear at the phase boundary, and to the presence or absence of a secondary FQ order in this phase. The present muon spin rotation and relaxation (μSR) study of $Ce_{0.75}La_{0.25}B_6$ is intended to provide new experimental information on this system via monitoring the local magnetic fields within phase IV and on crossing the different phase boundaries, either by varying T in zero external magnetic field and also in constant applied fields up to $B_{ext}=1.1$ T or at a fixed temperature by varying $\boldsymbol{B}_{ext}$.

The CsCl-type lattice structure of $Ce_xR_{1-x}B_6$ remains that of CeB_6, Fig. 1. The T-B phase diagram[28] for $x=0.75$ in Fig. 2 shows that, at this composition, for $B_{ext} \gtrsim 0.7$ T three phases exist, as in parent CeB_6. At lower B_{ext}, however, with the decrease of T phase I goes over to phase IV and *not* to phase II, which does not arise at all. The phase boundaries in the x-T plane[26,27] for $B_{ext}=0$, Fig. 2,[26] show that phase III is absent for zero field unless $x \gtrsim 0.7$. What happens is that for larger dilution phase IV extends down to $T=0$ in the B-T plane, "pushing" phase III up to higher-field regions. At $B_{ext}=0$, phase II exists only for $x \gtrsim 0.82$. The various transition temperatures are labeled as $T_{I\text{-}II}$, $T_{I\text{-}IV}$, $T_{II\text{-}III}$, and $T_{III\text{-}IV}$. No simple path exists to go directly from phase II to phase IV.

Before turning to the present knowledge on phase IV, we notice that even the identical nature of the magnetic order in the AFM phases III of $Ce_xLa_{1-x}B_6$ and CeB_6 is controversial. Although neutron diffraction patterns[31,32] and NMR[33] have not shown any significant qualitative difference between the magnetic structures, zero-field (ZF) μSR found eight distinct magnetic environments at the muon sites in pure CeB_6,[15] whereas in $Ce_{0.75}La_{0.25}B_6$ random static magnetic fields of $B \approx 300-500$ G were seen, in both phase III and phase IV.[34] Random fields of the order of $\approx$1000 G instead of a long-range order in phase IV were also seen in other ZF-μSR data.[35] It has been suggested[34] that the observed randomness is due to "frozen" ionic moments of $(0.13-0.16)\mu_B$.

Yet the specific heat anomaly[21] on entering phase IV does indicate some kind of long range order, even if, as neutron diffraction[32] suggests, not of a magnetic dipolar one. The possibility that the hidden order parameter in this phase is an octupole of type Γ_{5u} was discussed first in Ref. 39. After the discovery of a spontaneous, small trigonal lattice distortion ($\Delta L/L \approx 10^{-6}$) in phase IV[36] and in view of the strong softening of the shear constant c_{44} near the transition, it was suggested[37,40] that though the order is primarily magnetic octupole ordering, it is accompanied by an induced ferroquadrupolar (FQ) order of type $O_{yz}+O_{zx}+O_{xy}$. However, the antiferro-octupolar (AFO) and FQ order parameters alone cannot account for the strong random fields observed by ZF-μSR.

Most recently the direct observation of the octupolar order in phase IV of $Ce_{0.70}La_{0.3}B_6$ has been reported by use of RXS.[25] It was found that phase IV is indeed characterized by an AFO ordering of the f shells with wave vector $\boldsymbol{k}=\langle 1/2,1/2,1/2\rangle$ and that this order coexists with a mesoscopic short-range ($\approx$20–30 nm) AFM order of magnetic dipoles, with the same spatial period. The observed octupolar structure can account for the trigonal lattice distortion *even without* an induced quadrupolar order, which, in fact, was not seen in this experiment. The data also reveal the important fact that the mesoscopic order is not restricted to phase IV: the short-range AFM order was seen to be present also at $T\approx 3$ K in phase I, well above the temperature $T_{\text{I-IV}}=1.6$ K of the transition to phase IV. Thus, according to this experiment, it is the AFO order alone, segregated from the AFM component, that drives the transition. The observed short-range AFM order, on the other hand, explains both the presence of the spontaneous local fields seen earlier by ZF -μSR in phase IV and also their apparent randomness.

However, an important point in the above analysis of the RXS data was immediately challenged by a different interpretation.[24] Namely, the specific octupolar symmetry put forward for the AFO order in Ref. 25 is rejected, since, as the authors argue, an accurate evaluation of the same results exclude anything else than ordered Γ_{5u}-type octupole moments, predicted earlier by their theory.[39] They show that this predicted Γ_{5u}-type symmetry fits indeed well the data, with the additional assumption that four kinds of equally populated domains exist with alignments of the octupoles along one of the four equivalent cube diagonals. Further, in phase IV a coexisting electric FQ order is postulated and also an octupole-induced dipolar order which, in the presence of a slight and as yet unspecified crystalline disorder, could account for the observed short-range magnetic order. However, with this interpretation of octupole-induced magnetism it remains unclear why the magnetic structure appears to occur also *outside* phase IV in phase I. It has recently been also pointed out[41] that for a reliable identification of AFO order in phase IV further, more detailed RXS data are needed.

The present work extends previous preliminary μSR studies[34] on $Ce_{0.75}La_{0.25}B_6$ in ZF to studies in nonzero external fields, in both longitudinal field (LF) and transverse field (TF) geometries. The former allows one to investigate dynamical aspects, the latter to measure the μ^+ Knight shift and static internal hyperfine field distributions in the different phases of this compound. While the very-short-ranged octupole fields of a Ce^{3+} ion are necessarily difficult to detect at the distance of the interstitial μ^+ site, and so an octupolar order parameter remains hidden for μSR, these experiments still give relevant information also on phase IV by signaling the variation of the static and dynamical behavior of the concomitant *dipolar* fields present in this state.

Earlier not so systematic ZF, TF, and LF studies were performed by another group on a $Ce_{0.70}La_{0.3}B_6$ single-crystal sample.[35]

The paper is organized as follows.

Section II reports on the experimental details. Section III deals with TF measurements above 10 K which allowed us to determine the μ^+ site and identify the nearest-neighbor Ce or La configuration. From previous studies on CeB_6 it is known that the μ^+ reside at the interstitial d sites,[16] Fig. 1, which are occupied also in the present compound. Section IV describes and discusses the ZF results in more detail than in Ref. 34; an unexpected observation is the appearance of a spatial segregation into magnetic and nonmagnetic volume fractions in phase IV. Section V describes and discusses the TF results in phases II, III, and IV. It will be seen that, while the Knight shifts do not reflect the various phase transitions and phases, the inhomogeneity of the internal field is clearly modified at the I-IV and III-IV phase boundaries. In contrast, the I-II and II-III transitions are only weakly if at all manifest in the field inhomogeneity. Section VI describes and discusses the μ^+ spin lattice relaxation in LF geometry. The I-IV and III-IV transitions lead to pronounced singularities, as does the II-III transition and less strongly the I-II transition. Finally, Sec. VII provides conclusions and a summary.

II. EXPERIMENTAL DETAILS

The μSR-measurements were performed at the Swiss Muon Source (SμS) of the Paul Scherrer Institut using the General Purpose Instrument (GPS) for the high temperature Knight shift measurements and the Low Temperature Facility (LTF) for zero field and transverse+longitudinal field measurements across the phase diagram below 4 K, both on the surface μ^+ beam line πM3. The LTF allows one to apply temperatures down to 20 mK and magnetic fields B_{ext} up to 3 T. In the transverse field (TF) measurements, the initial μ^+ polarization $\mathbf{P}_\mu(0)$ was rotated from being parallel to the beam momentum and the applied field by $\sim$50° toward the vertical axes by means of a spin rotator. This allowed us to monitor the μ^+ Larmor precession, in positron detectors, oriented perpendicular to the beam axis (in up, down, and right directions in the GPS, in left, right directions in the LTF) and simultanously, the depolarization of the μ^+ spin-polarization component [$\propto\cos(50°)$] along the applied field in forward and backward placed detectors [longitudinal field (LF) configuration]. Two single crystal samples of $Ce_{0.75}La_{0.25}B_6$ were used in the experiment. The first one had the shape of cylinder (ϕ3.8 mm, length 7.7 mm), with the cylinder axis parallel to a $\langle 001\rangle$ axis. The second sample consisted of three 1 mm thick flat plates covering an area of approximately 5 $\times$ 14 mm^2. The plate normal was parallel to a $\langle 110\rangle$ axis. Both samples were prepared by Professor S. Kunii at the Tohoku University, Sendai, Japan, by a floating zone method. The first sample was used in the GPS, where it could be rotated inside a He-flow cryostat around the cylinder axis oriented perpendicular to the applied field that is parallel to the beam axis. Hence, the orientation of the applied field could be turned in the (001) plane, and it was possible to study in particular the orientation $\mathbf{B}_{\text{ext}}\|\langle 110\rangle$ axis and $\mathbf{B}_{\text{ext}}\|\langle 100\rangle$ axis. The second sample was used in the LTF, where the three plates were glued to a silver sample holder. In this case only the orientation $\mathbf{B}_{\text{ext}}\|\langle 110\rangle$-axis could be studied. While in the GPS, practically only positrons emerging from μ^+ stopped in the sample made up the μSR signal. In the LTF, about 30% originated from μ^+ stopped outside the sample in the silver holder. This was not an undesired feature, since it allowed us to determine the strength of the

applied field from the precession frequency of this background μSR signal. Further, the closeness of the μ^+ stopped around outside of the sample rendered them susceptible to the magnetization of the sample which produced a certain field inhomogeneity, which should be proportional to the sample magnetization and determines the relaxation rate of the background signal by dephasing. This feature allowed us to monitor the temperature and field dependence of the sample magnetization or susceptibility, which was not available from the literature in all cases covered here by the experiments.

As usual in a μSR experiment the evolution of the μ^+ polarization $\boldsymbol{P}_\mu(t)$ is monitored via the time-dependent decay asymmetry of nearly 100% spin-polarized implanted μ^+ by observing the positrons from the μ^+ decay in a certain direction $\boldsymbol{r}$ as a function of the elapsed μ^+ lifetime. The positron rate can then be written as[42]

$$\frac{dN_{e^+}(t)}{dt} = \frac{1}{4\pi\tau_\mu} N_0 e^{-t/\tau_\mu}(1 - a\boldsymbol{P}_\mu(t)\cdot\boldsymbol{r})\Omega_r, \tag{1}$$

where a is the effective decay asymmetry (0.2–0.3), τ_μ the mean muon lifetime (2.2 μs), $|\boldsymbol{r}|=1$, and Ω_r the solid angle covered by the detector in the direction $\boldsymbol{r}$. In the following we will call $aP(0)\equiv a\boldsymbol{P}_\mu(0)\cdot\boldsymbol{r}$ asymmetry or (signal) amplitude.

III. KNIGHT SHIFT MEASUREMENTS IN PARAMAGNETIC PHASE I

A. Experimental results

The measurements in PM phase I were performed at $\boldsymbol{B}_{\text{ext}}=0.6$ T using the cylindrical sample in the GPS. The accumulated TF spectra in up, down, and right detectors revealed up to six different precession frequencies, each signal decaying by a Gaussian damping function. Hence $aP(t)$ is given by

$$aP(t) = \sum_{i=1}^{6} a_i \exp\left(-\frac{1}{2}\sigma_i^2 t^2\right)\cos(\omega_i t + \varphi), \tag{2}$$

with $\Sigma_{i=1}^6 a_i = a$, where $\omega_i = \gamma_\mu B_\mu = 2\pi\nu_i$, B_μ is the local field at the μ^+ site, $\gamma_\mu = 2\pi \times 13.5539$ kHz/G is the muon's gyromagnetic ratio, and σ_i are the Gaussian decay rates, where σ_i is related to the spread ΔB in local fields: $\sigma_i = \gamma_\mu \Delta B$. The phase φ is the same for all components and depends on the detector directions $\boldsymbol{r}$. The splitting of the precession frequencies can be made visible by Fourier transforming the accumulated spectra. As an example, Fig. 3 shows the Fourier (power) spectrum obtained from data taken at 10 K with $\boldsymbol{B}_{\text{ext}}$ and the $\langle 100\rangle$ axis enclosing an angle of $\sim 25°$. The lowest-frequency signal is actually composed of two components (ν_5, ν_6), which are not separately visible in the Fourier spectra but can be resolved by analyzing the the original time spectra. Since the latter splitting is always small and decreases further with increasing temperature, we mostly ignore the splitting and restrict the analysis to five components—i.e., $\nu_6 \simeq \nu_5$. Following this procedure Fig. 4 shows the orientation dependence of the five frequencies as

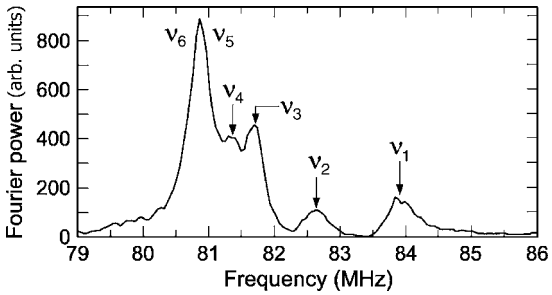

FIG. 3. Fourier transform of the TF-μSR signal at 10 K and $B_{\text{ext}}=0.600$ T (corresponding to a precession frequency of 81.323 MHz). The sample was oriented such that the angle between $\mathbf{B}_{\text{ext}}$ and the $\langle 100\rangle$ axis was close to 25°. The signal is split into a maximum of six components.

the sample is turned around the cylinder axis. The angular dependences are described perfectly by the following expressions:

$$\nu_1 = \bar{\nu}_1 + \nu_1^{(2)} \cos 2\varphi, \tag{3a}$$

$$\nu_3 = \bar{\nu}_3 - \nu_3^{(2)} \cos 2\varphi, \tag{3b}$$

$$\nu_2 = \bar{\nu}_2 + \nu_2^{(2)} \cos 2\varphi, \tag{3c}$$

$$\nu_4 = \bar{\nu}_4 - \nu_4^{(2)} \cos 2\varphi, \tag{3d}$$

$$\nu_6 = \nu_5 = \text{const}, \tag{3e}$$

where φ is the angle between $\boldsymbol{B}_{\text{ext}}$ and the $\langle 100\rangle$ axis. The fit shows that $\bar{\nu}_1 = \bar{\nu}_3$, $\nu_1^{(2)} = \nu_3^{(2)}$, $\bar{\nu}_2 = \bar{\nu}_4$, and $\nu_2^{(2)} = \nu_4^{(2)}$. Apparently ν_1, ν_3 and ν_2, ν_4, respectively, are closely related. The analysis reveals further that the components can be grouped into two sets within which the amplitudes are the same. The sets comprise the frequencies ν_1, ν_3, ν_5 and ν_2, ν_4, ν_6, respectively. The amplitude in the first set is roughly 1.7 times

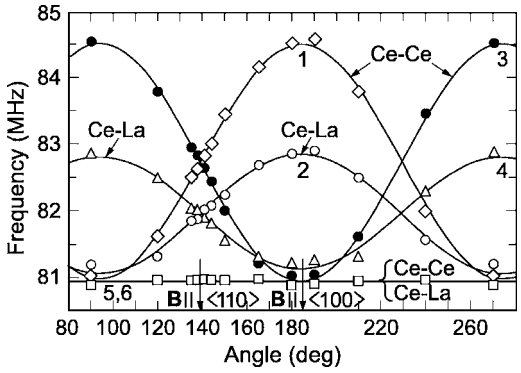

FIG. 4. Orientation dependence of the six precession frequencies at 10 K when rotating the sample around the $\langle 001\rangle$ axis, perpendicular to $\mathbf{B}_{\text{ext}}$. $\mathbf{B}_{\text{ext}}$ is confined to the (001) plane. The nearly coinciding frequencies ν_5 and ν_6 show no angular dependence. The solid lines represent fits of Eq. (3) to the data. Components 1, 3, and 5 originate from μ^+ with two Ce atoms as nearest neighbors, components 2, 4, and 6 from μ^+ with one Ce and one La atom as nearest neighbors; see Sec. III B.

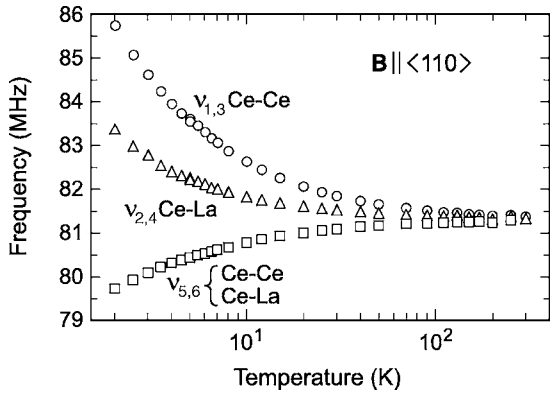

FIG. 5. Temperature dependence of the precession frequencies $\nu_{1,3}$, $\nu_{2,4}$, and $\nu_{5,6}$ for $\mathbf{B}_{\text{ext}}\|\langle 110\rangle$ axis. For this orientation $\nu_3=\nu_1 \equiv \nu_{1,3}$ and $\nu_4=\nu_2\equiv\nu_{2,4}$. The nearly coinciding frequencies ν_5, and ν_6 are replaced by their average $\nu_{5,6}$.

larger than the amplitude in the second set. Figure 4 shows that $\nu_1=\nu_3$ and $\nu_2=\nu_4$ for $\boldsymbol{B}_{\text{ext}}\|\langle 110\rangle$ and $\nu_3=\nu_5$ and $\nu_4=\nu_6$ for $\boldsymbol{B}_{\text{ext}}\|\langle 100\rangle$; hence, the number of components reduces to 3. For $\boldsymbol{B}_{\text{ext}}\|\langle 110\rangle$, $aP(t)$ may be written (neglecting the phases)

$$aP(t) = 2a_1 \exp\left(-\frac{1}{2}\sigma_{1,3}^2 t^2\right)\cos\,\omega_{1,3}t + 2a_2 \times\exp\left(-\frac{1}{2}\sigma_{2,4}^2 t^2\right)\cos\,\omega_{2,4}t + (a_1+a_2) \times\exp\left(-\frac{1}{2}\bar{\sigma}_{5,6}^2 t^2\right)\cos\,\bar{\omega}_{5,6}t, \tag{4}$$

and, for $\boldsymbol{B}_{\text{ext}}\|\langle 100\rangle$,

$$aP(t) = a_1 \exp\left(-\frac{1}{2}\sigma_1^2 t^2\right)\cos\,\omega_1 t + a_2 \exp\left(-\frac{1}{2}\sigma_2^2 t^2\right)\cos\,\omega_2 t + 2(a_1+a_2)\exp\left(-\frac{1}{2}\bar{\sigma}_{3,4,5,6}^2 t^2\right)\cos\,\bar{\omega}_{3,4,5,6}t, \tag{5}$$

where $\omega_{i,j}\equiv\omega_i=\omega_j$, $\sigma_{i,j}\equiv\sigma_i=\sigma_j$, etc., and $\bar{\omega}_{i,\ldots}$ and $\bar{\sigma}_{i,\ldots}$ are to be understood as properly weighted averages.

In general, the number of components in $Ce_{0.75}La_{0.25}B_6$ is *twice* the number of components seen in CeB_6, suggesting that two different types of equivalent μ^+ positions are involved in $Ce_{0.75}La_{0.25}B_6$.

In order to determine the μ^+ positions and to learn about other possible differences with respect to CeB_6, we apply the usual procedure by measuring the μ^+ Knight shift as a function of temperature for different orientations,[43] in the present case for $\boldsymbol{B}_{\text{ext}}\|\langle 100\rangle$ and $\boldsymbol{B}_{\text{ext}}\|\langle 110\rangle$, and analyzing the spectra with Eqs. (4) and (5). The fitted frequencies $\nu_{1,3}$, $\nu_{2,4}$ and $\bar{\nu}_{5,6}$ for $\boldsymbol{B}_{\text{ext}}\|\langle 110\rangle$ are displayed in Fig. 5. One finds that $\nu_1(T)$, $\nu_3(T)$, and $\nu_5(T)$ agree perfectly with the corresponding frequencies in CeB_6,[16,17] suggesting that the set of frequencies ν_1, ν_3, and ν_5 originate from μ^+ which reside at the magnetically inequivalent d sites as in CeB_6 with only Ce atoms as nearest neighbors.

B. Discussion of TF results in phase I and comparison with CeB_6

To proceed further, the Knight shift of the observed precession frequencies has to be considered.[43] The Knight shift, we recall, consists of a dipolar and a contact hyperfine contribution: the former arises from the dipole fields at the μ^+ sites originating from the field-induced magnetic moments on the Ce sites, the latter from the conduction electron spin polarization at the μ^+ position which, via the RKKY interaction, is also induced by the Ce $4f$ moments. The fact that the number of components per set is 3, like in CeB_6, is consistent with the conjecture that also in $Ce_{0.75}La_{0.25}B_6$ the μ^+ is found at the d sites, which for an arbitrary direction of $\boldsymbol{B}_{\text{ext}}$ with respect to the crystal axes separate into three magnetically inequivalent subsites: e.g., the sites $(\frac{1}{2}00)$, $(0\frac{1}{2}0)$, and $(00\frac{1}{2})$. The dipolar contribution to the Knight shift constant K is given by the general expression[43]

$$K_{dip} = \boldsymbol{b}\overleftrightarrow{A}_{dip}\overrightarrow{\chi}\boldsymbol{b}, \tag{6}$$

where $\boldsymbol{b}=\boldsymbol{B}_{\text{ext}}/B_{\text{ext}}$, $\overleftrightarrow{A}_{dip}$ is the dipolar coupling tensor with $\text{tr}\overleftrightarrow{A}_{dip}=0$, and $\overrightarrow{\chi}$ is the magnetic susceptibility tensor, which in cubic CeB_6 is a scalar.

In the case of the d sites in CeB_6, $\overleftrightarrow{A}_{dip}$ is diagonal and for the site $(00\frac{1}{2})$ reads

$$\overleftrightarrow{A}_{dip}^{(0\ 0\ 1/2)} = \begin{pmatrix} -\frac{1}{2}A_{dip} & 0 & 0 \\ 0 & -\frac{1}{2}A_{dip} & 0 \\ 0 & 0 & A_{dip} \end{pmatrix}. \tag{7}$$

For the two other sites the diagonal elements have to be interchanged. Confining $\boldsymbol{B}_{\text{ext}}$ to the (001) plane, as in our experiment, the angular dependence of K for the d sites reads, including now also a contact coupling parameter A_c,

$$K^{(0\ 0\ 1/2)}(\varphi) = \left[A_c(\varphi) - \frac{1}{2}A_{dip}\right]\chi, \tag{8a}$$

$$K^{(0\ 1/2\ 0)}(\varphi) = \left[A_c(\varphi) + \left(\frac{1}{4} - \frac{3}{4}\cos 2\varphi\right)A_{dip}\right]\chi, \tag{8b}$$

$$K^{(1/2\ 0\ 0)}(\varphi) = \left[A_c(\varphi) + \left(\frac{1}{4} + \frac{3}{4}\cos 2\varphi\right)A_{dip}\right]\chi, \tag{8c}$$

where φ is the angle between $\boldsymbol{B}_{\text{ext}}$ and the $\langle 100\rangle$ axis. Usually the contact coupling parameter is considered to be isotropic and temperature independent. However, as previous studies of CeB_6 have revealed,[16,17] A_c is also anisotropic and $A_c(\varphi)$ for the different sites follows the same angular dependence as $K_{dip}(\varphi)$.[34] Comparing the experimental fits, Eqs. (3) and (8), it is seen that the d-site assignment reproduces correctly the measured angular dependence of the precession frequencies also for $Ce_{0.75}La_{0.25}B_6$.

The final proof for the site assignment follows from the temperature dependence of the Knight shifts for $\boldsymbol{B}_{\text{ext}}\|\langle 100\rangle$ and $\boldsymbol{B}_{\text{ext}}\|\langle 110\rangle$. To analyze this, first it is clear that with the

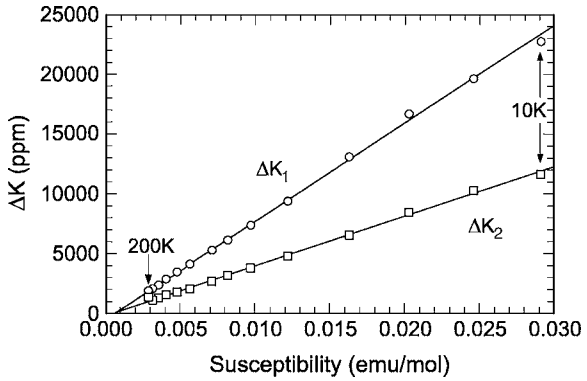

FIG. 6. Plot of $\Delta K_1=[\nu_1(\mathbf{B}_{\text{ext}}\|\langle 100\rangle)-\nu_1(\mathbf{B}_{\text{ext}}\|\langle 110\rangle)]/\nu_{\text{ext}}$ and $\Delta K_2=[\nu_2(\mathbf{B}_{\text{ext}}\|\langle 100\rangle)-\nu_2(\mathbf{B}_{\text{ext}}\|\langle 110\rangle)]/\nu_{\text{ext}}$ versus the bulk magnetic susceptibility $\left(\nu_{\text{ext}}=\frac{\gamma_\mu}{2\pi}B_{\text{ext}}\right)$. These Knight shift differences are free of the macroscopic contributions of Lorentz field and demagnetization field. ΔK_1 and ΔK_2 scale perfectly with the bulk magnetization in the covered temperature range. The solid straight lines represent fits of Eq. (9) to the data.

solute atoms in the lattice, Eq. (7) is in general no more valid, since the high local symmetry of the d sites present in CeB_6 is now lost. In the ternary compound each d site has a different $\overleftrightarrow{A}_{dip}$ tensor, corresponding to the actual atomic configuration of its environment. However, limiting ourselves to the nearest-neighbor atoms, the by far most important sources of the local field, the number of different dipole tensors reduces to 3: namely, for zero, one, or two La neighbors. In this case the diagonal form, Eq. (7), of $\overleftrightarrow{A}_{dip}$ is still valid due to the collinear configuration, and the statistical weights for zero, one, and two La neighbors are 0.5625, 0.375, and 0.0625, respectively. As seen below, the Knight shift data can be well understood by this nearest neighbor-approximation.

The actual extraction of the Knight shifts from the precession frequencies requires one to correct the measured shifts for the demagnetization and Lorentz field contributions. We circumvent this procedure by calculating $\Delta K_1=[\nu_1(\boldsymbol{B}_{\text{ext}}\|\langle 100\rangle)-\nu_1(\boldsymbol{B}_{\text{ext}}\|\langle 110\rangle)]/\nu_{\text{ext}}$ and $\Delta K_2=[\nu_2(\boldsymbol{B}_{\text{ext}}\|\langle 100\rangle)-\nu_2(\boldsymbol{B}_{\text{ext}}\|\langle 110\rangle)]/\nu_{\text{ext}}$ which eliminates the demagnetization and Lorentz field contributions since χ is isotropic and the demagnetization factor independent of the direction of $\boldsymbol{B}_{\text{ext}}$ which is always perpendicular to the cylinder axis. The quantities ΔK_1 and ΔK_2 are plotted in Fig. 6 versus the bulk magnetic susceptibility of $Ce_{0.75}La_{0.25}B_6$, taken from Ref. 44. We find a strictly linear relation down to 10 K. We fit the data above 10 K by the expression, Eq. (6),

$$\Delta K_i = A_i(\chi-\chi_0), \quad i=1,2, \tag{9}$$

where χ_0 is a temperature-independent contribution, usually related to the Pauli spin susceptibility of the conduction electrons, and $\chi-\chi_0=\chi_{4f}$ is the susceptibility of the $4f$ electrons.

The results are collected in Table I. As can be seen A_2 is rather precisely half the value of A_1. Below 10 K the linear scaling is lost.

Equation (8c) implies that

TABLE I. Collection of fitted χ_0 and A_i.

i	χ_0 (10^{-4} emu)	A_i (kG/μ_B)
1	8.0 (0.5)	4.52(3)
2	4.4 (1.6)	2.27 (5)

$$A_1=\left(A_c(\varphi=0)-A_c(\varphi=45^\circ)+\frac{3}{4}A_{dip}\right). \tag{10}$$

We can calculate the corresponding quantity for CeB_6 from the results in Refs. 16 and 17. With $A_c(\varphi=0)=3.95$ kG/μ_B, $A_c(\varphi=45^\circ)=2.475$ kG/μ_B, and $A_{dip}=3.94$ kG/μ_B we find $A_1=4.43$ kG/μ_B which coincides almost perfectly with the fitted $A_1=4.52$ kG/μ_B. It proves that the μ^+ which generate the frequencies ν_1, ν_3, and ν_5 are indeed located at d sites, where both nearest-neighbor host atoms must be Ce atoms. Since $A_2=0.5A_1$, it is concluded that the μ^+ which generate the frequencies ν_2, ν_4, and ν_6 are as well located at the d sites but one nearest Ce neighbor is replaced by a nonmagnetic La atom. Sites where both nearest neighbors are La atoms are not visible due to their low statistical weight. The ratio of the signal amplitudes, a_1/a_2, is approximately 1.76 ± 0.09, which means that the probability for the μ^+ to find one Ce and one La atom as nearest neighbors is 0.34 ± 0.01, in good agreement with the expected 37%. For temperatures below ~5 K the Ce-La nearest-neighbor configuration becomes less probable and seems to depend on both the temperature and the strength of the applied field. This feature is not yet understood.

The agreement of A_1 with the corresponding value in CeB_6 implies also that the contact coupling constant A_c and its anisotropy in $Ce_{0.75}La_{0.25}B_6$ are unchanged and numerically the same as in CeB_6, given that A_{dip} for the Ce-μ^+-Ce configuration has to be the same in both compounds, neglecting small differences due to slightly different lattice constants. Since A_c involves the RKKY interaction,[34] one can claim that the electronic properties of the Ce^{3+} ions and the conduction electron systems are the same in both compounds. The anisotropy of A_c in CeB_6 has previously been explained as arising from a field-induced ordering of the quadrupole moments of the $4f$-electron charge distribution (field-induced ferroquadrupolar ordering), affecting the RKKY coupling.[17] The present results imply that this explanation can be carried over to $Ce_{0.75}La_{0.25}B_6$ and that the incorporation of magnetic holes into the Ce sublattice, at least above 10 K, does also not affect the quadrupolar properties of the Ce ions.

IV. ZERO-FIELD MEASUREMENTS IN PHASES I, IV, AND III

A. Experimental results

From 100 mK (lowest temperature applied) up to the boundary between phases III and IV ($\simeq$1.3K) the signal shows the presence of two components described by the expression

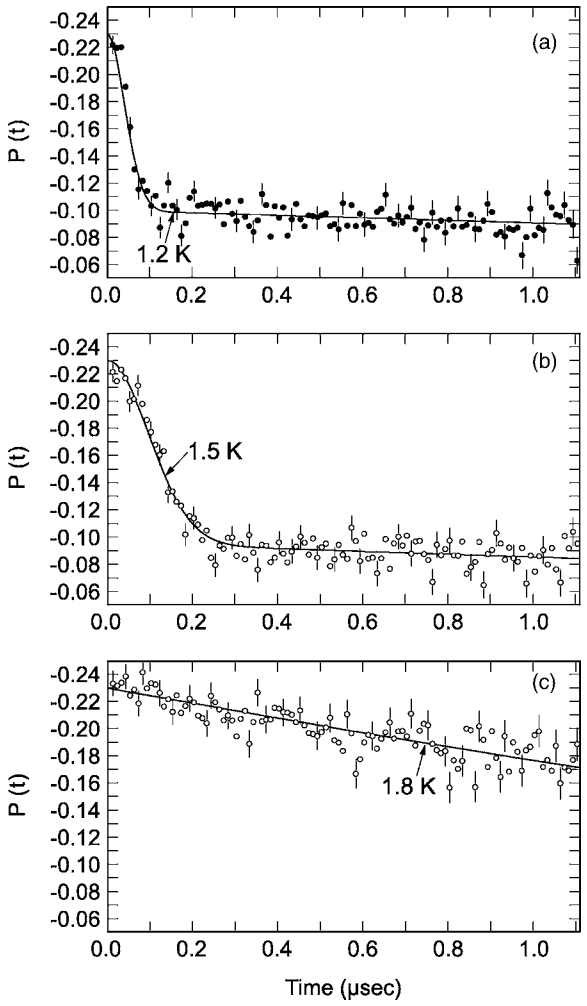

FIG. 7. ZF signals $P(t)$ at (a) 1.2 K in phase III, (b) at 1.5 K in phase IV, and (c) at 1.8 K in phase I. The solid lines represent fits of Eqs. (11)–(13), respectively to the data. The orientation of the sample was $\mathbf{P}_\mu(0) \| \langle 110 \rangle$ axis.

$$aP(t) = a_1 \exp\left(-\frac{1}{2}\sigma^2 t^2\right) + a_2 \exp(-\lambda t), \tag{11}$$

with amplitudes (asymmetries) $a_1/a_2 = 2$ or $a_1 = \frac{2}{3}a$, respectively. In phase IV up to the boundary to phase I ($\simeq 1.65$K) a third essentially time-independent (as far as we can tell) signal grows from zero up to 100%—i.e.,

$$aP(t) = a_{12}\left[\frac{2}{3}\exp\left(-\frac{1}{2}\sigma^2 t^2\right) + \frac{1}{3}\exp(-\lambda t)\right] + a_3, \tag{12}$$

such that $a_{12} + a_3 = a$. Then, in phase I, the signal changes to

$$aP(t) = a\exp(-\lambda t)\exp\left(-\frac{1}{2}\sigma^2 t^2\right). \tag{13}$$

Corresponding fitted signals are displayed in Fig. 7, the fitted asymmetries a_i, Gaussian relaxation rates σ, and exponential relaxation rates λ in Fig. 8.

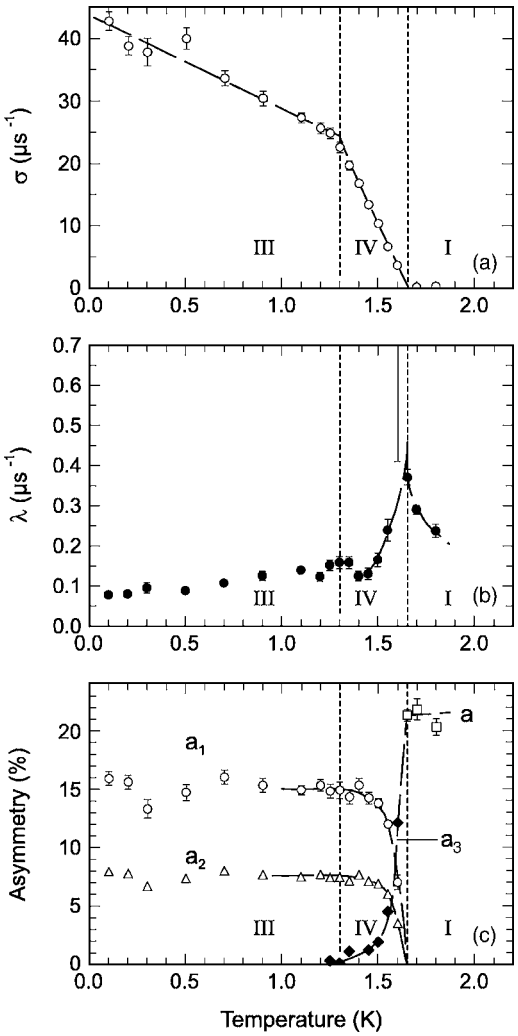

FIG. 8. Temperature dependence of the zero-field Gaussian (a) and exponential (b) relaxation rates σ and λ. Panel (c) shows the temperature dependence of the corresponding signal amplitudes a_1, a_2, and a_3. Note that $a_3 \neq 0$ only in phase IV.

B. Discussion of ZF results

The form of the signal, Eq. (11), in phase III indicates that the μ^+ is exposed to randomly oriented static and fluctuating internal magnetic fields. In this situation one expects a dynamic Kubo-Toyabe function[45] or, if the fluctuations are slow, a modified static Kubo-Toyabe function, in which the 1/3 term decays exponentially with a rate $\lambda \simeq \frac{2}{3}\nu$, where ν is the fluctuation rate.[45] The observed $P(t)$ comes close to the latter function, except that the characteristic minimum in $P(t)$ is missing. We explain this feature, which is often also observed in other frustrated magnetic compounds, to arise from a spatially inhomogenously distributed field spread, experienced by the muons which washes out the minimum in $P(t)$. In any case the dominating Gaussian relaxation implies a Gaussian-distributed spread of the internal static fields $\boldsymbol{B}_\mu$ at the μ^+ sites. At 100 mK, $\sigma \simeq 43\ \mu s^{-1}$ which translates into a field spread of $\Delta B = \sigma/\gamma_\mu \simeq 500$ G. The I-IV and IV-III phase boundaries are well reflected in σ and the asymmetries, Fig. 8. The relaxation rate λ tends to diverge at the

transition temperature $T_{I\text{-}IV}$, showing a cusplike singularity similar to that seen in earlier NMR work.[46] The Gaussian relaxation rate σ displays a kind of linear temperature dependence with a clear break of the slope at the III-IV phase boundary.

In phase IV the maximum $\sigma \simeq 25\ \mu s^{-1}$ corresponds to a field spread of 290 G and clearly indicates that also phase IV involves a random or short-range magnetic order of the Ce $4f$-dipole moments. Interestingly though, as shown by the appearance of a third component, the magnetic volume fraction grows from zero at the IV-I phase boundary and approaches 100% at the IV-III phase boundary; i.e., within the phase IV, a certain phase separation is evident. Otherwise the qualitative behaviors of the magnetic signals in phase IV and phase III are so similar that the type of dipolar magnetic structure, as seen by μSR, in phases III and IV appears to be essentially the same, as also indicated by NMR work[46] (see also Sec. V B).

The observation of a nonzero λ in phases III and IV indicates that the magnetic order is not purely static but some residual fluctuations of the moments must take place. It is tempting to interpret λ to directly reflect the fluctuation rate ν, $\lambda = \frac{2}{3}\nu$, as introduced earlier, which then would be of the order of 0.2 MHz. Such a slow rate is, however, incompatible with the longitudinal field results, to be discussed in Sec. VI. Rather the fluctuation rates must be fast. If the full moment were to fluctuate very rapidly, the dynamic Kubo-Toyabe function would convert to a simple exponential function with full amplitude and a small relaxation rate, which clearly is not observed. However, the observed behavior can be understood if, in addition to static fields, a different source of fluctuating fields is present. In this case the expected relaxation function is given by the expression (two-channel relaxation)

$$P(t) = f_{KT}(t)\exp(-\lambda t), \tag{14}$$

where $f_{KT}(t)$ is the static Kubo-Toyabe function[45]

$$f_{KT}(t) = \frac{1}{3} + \frac{2}{3}(1-\Delta^2 t^2)\exp\left(-\frac{1}{2}\Delta^2 t^2\right). \tag{15}$$

If $\lambda \ll \Delta$ and the minimum in $f_{KT}(t)$ is ignored for the reasons outlined above, Eq. (11) is recovered.

The fluctuating fields may be associated with isolated single Ce^{3+} spins which are not taking part in the magnetic order or with a small-amplitude vibration of the Ce^{3+} spins around some fixed direction with a large static amplitude along this direction. We prefer the first possibility in view of the apparent formation of paramagnetic domains in phase IV. It is also evident from Fig. 8(b) that the dynamics is not changing noticeably when passing from phase III to phase IV, consistent with the view that the magnetism in both phases is essentially the same. Therefore, the difference between phase III and phase IV, as seen by μSR in *zero field* (i.e., apart from the octupolar order in phase IV), is that in phase IV the volume separates into dipolar magnetic and nonmagnetic domains.

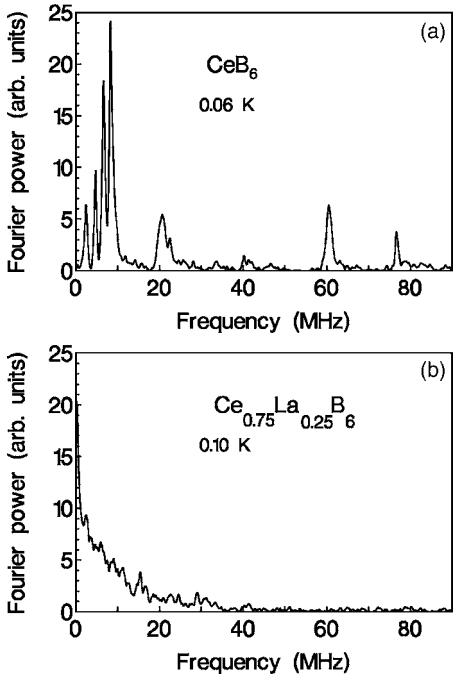

FIG. 9. Fourier transform (power) of the ZF-μSR signal in phase III in (a) CeB_6 at 0.06 K (from Ref. 15) and (b) $Ce_{0.75}La_{0.25}B_6$ at 0.1 K.

If we interpret σ as arising from a random spin-glass-like freezing of the Ce moments, we can calculate the expected second moment of the resulting field spread at the d sites, which amounts to $M_2 = 6.63 \times 10^{16}\ s^{-2}/\mu_B^2$ or $\sigma = 2.57 \times 10^8\ s^{-1}/\mu_B$ for the CeB_6 lattice. Comparing the latter value with the experimental σ we find that the magnitude of the average frozen moments amount to $0.18\mu_B$ at 100 mK and to $0.10\mu_B$ at 1.3 K.

Our results in phase III do not confirm a long-range AFM order as claimed to be found by a neutron powder diffraction study[32] carried out in $Ce_{0.75}La_{0.25}B_6$. According to that work the antiferromagnetic structure in phase III is very similar to the structure found in CeB_6 in phase III.[9] Using the model C of Ref. 9, the ordered moments are estimated to be $\mu_{Ce(1)} = 0.53\mu_B$ and $\mu_{Ce(2)} = 0.12\mu_B$ at 105 mK, slightly smaller or of similar magnitude as in CeB_6. We recall that in CeB_6 the μSR signal in phase III revealed *eight* distinct spontaneous frequencies[15] [see the Fourier transform in Fig. 9(a)], corresponding to internal fields between 180 G and 5.6 kG at 60 mK. Performing the same Fourier transformation on the ZF signal in $Ce_{0.75}La_{0.25}B_6$ at 0.1 K [lowest temperature applied, Fig. 9(b)] we find only a broad peak at zero frequency which just reflects the Fourier transform of the Gaussian damped signal displayed in Fig. 7. No distinct frequencies can be seen in striking contrast to the situation in CeB_6. Further, if the magnetic order in phase III of $Ce_{0.75}La_{0.25}B_6$ possessed the same structure as in the CeB_6, but were highly disturbed or short ranged due to the presence of the La magnetic holes, we should have expected that the total field spread experienced by the μ^+ would be much larger than the 500 G found in the experiment; in fact, the signal should be wiped out. Also it is not evident that the field spread should

be represented by a perfect Gaussian distribution.

We will see in the next section that the TF results are likewise in conflict with a long-range AFM order in phase III.

Concerning phase IV, the neutron study does not find any evidence for magnetic order. Resonant x-ray scattering, on the other hand, seems to show a short-range (20–30 nm) AFM order involving the Ce 5*d* electrons.[25] Moreover, this order is claimed to develop already below 3 K. While the present ZF-μSR results do not provide any evidence for magnetic order above phase IV, they may support the suggested short-range AFM order in phase IV. A short-range or mesoscopic order may also explain the absence of any detectable magnetic Bragg peak in the neutron data.

The evidence for persisting magnetic order above $T_{I\text{-}IV}$ up to ~3K from the RXS measurements and the absence of such evidence in the μSR data may find its explanation in the different time windows of the two techniques. Thus AFM correlations with short correlation times may appear static in the RXS measurements but highly dynamic to the muon. However, the same argument cannot be used to explain the inconsistency of the neutron and μSR data in phase III.

V. TRANSVERSE FIELD MEASUREMENTS IN PHASES I, II, III, AND IV

A. Experimental results

TF measurements were performed at B_{ext}=0.3 T in the temperature range of 1–2.5 K, allowing one to cross from phase III to phase IV to phase I, and at 1.1 T in the range of 1.4–4 K, allowing one to cross from phase III to phase II and further to phase I. The applied field was always oriented parallel to a ⟨110⟩ axis. Independent of temperature and field strength, the TF data revealed always three precession frequencies as in phase I at higher temperatures (see Sec. III). The data could be well fitted by Eq. (4) with the Gaussian decay of the precession signals leading to best fits also in phases II, III, and IV. Note that the lowest-frequency component for $\boldsymbol{B}_{\text{ext}}\|\langle 110\rangle$, as described in Sec. III, consists of two components with frequencies ν_5 and ν_6 which are nearly indistinguishable and are replaced by the average $\nu_{5,6}$. Correspondingly the Gaussian decay rates σ_5 and σ_6 are replaced by the average $\sigma_{5,6}$. Frequencies $\nu_{1,3}$ and $\nu_{2,4}$ and decay rates $\sigma_{1,3}$ and $\sigma_{2,4}$ are defined as in Eq. (4). Note that in phase IV the TF signal does not reflect the appearance of different domains as seen in the ZF signal.

The temperature dependence of the fitted precession frequencies $\nu_{1,3}$, $\nu_{2,4}$, and $\nu_{5,6}$ and Gaussian decay rates $\sigma_{1,3}$, $\sigma_{2,4}$, and $\sigma_{5,6}$ are displayed in Fig. 10 (0.3 T) and Fig. 11 (1.1 T). In fitting the TF spectra from the field scan at 1.5 K we noticed that $\sigma_{5,6}\simeq\sigma_2$ and in the final round of fits used the relation $\sigma_{5,6}=\sigma_{2,4}$. The corresponding results are displayed in Fig. 12(a).

The fits included, as already pointed out, a further component arising from μ^+ stopping in the silver sample holder. The damping of this component is a measure of the field inhomogeneity experienced by these μ^+, which in turn is proportional to the sample magnetization. The field dependence of the inhomogeneity, expressed as a frequency spread $\Delta\nu_{BG}$, is shown in Fig. 12(c).

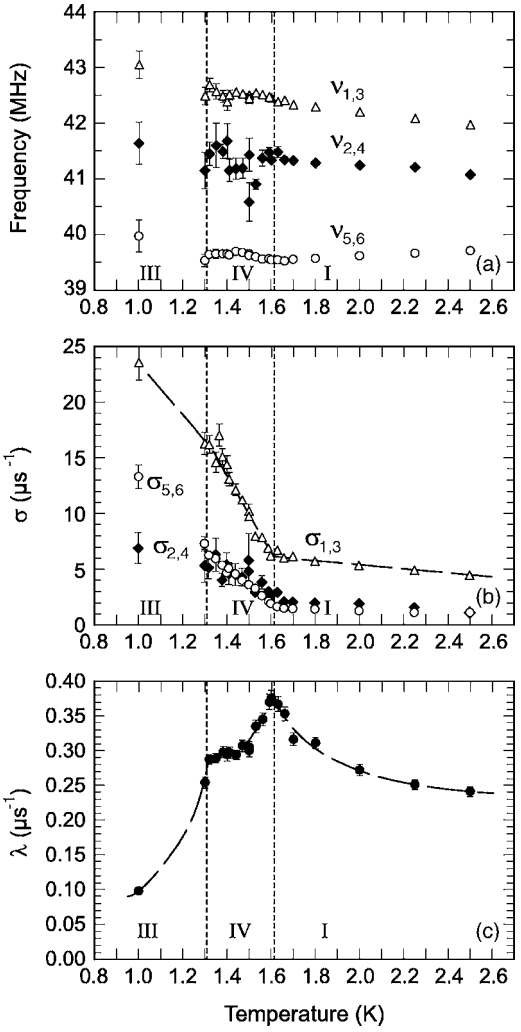

FIG. 10. Temperature dependence of the fitted parameters (a) $\nu_{1,3}$, $\nu_{2,4}$, and $\nu_{5,6}$, (b) $\sigma_{1,3}$, $\sigma_{2,4}$, and $\sigma_{5,6}$, and (c) λ from the 0.3 -T runs. Note the absence of any clear anomalies of the precession frequencies at $T_{I\text{-}IV}$ and $T_{III\text{-}IV}$, in contrast to the behavior of the Gaussian relaxation rate σ and the LF exponential relaxation rate λ.

B. Discussion of the TF results

Inspecting Fig. 10 we notice a rather weak temperature dependence of $\nu_{1,3}$, $\nu_{2,4}$, and $\nu_{5,6}$ with no visible anomalies at $T_{I\text{-}IV}$ and $T_{IV\text{-}III}$. The same behavior is also seen at 1.1 T, no anomalies at $T_{I\text{-}II}$ and $T_{II\text{-}III}$, in particular no further splitting occurs in phase III; see Fig. 11. This is again in striking contrast to the behavior seen in CeB_6. Figure 13 displays the temperature dependence of the precession frequencies observed in CeB_6 at 0.6 T with $\boldsymbol{B}_{\text{ext}}\|\langle 110\rangle$. Above T_N we see the two expected frequencies for this field orientation, but immediately below T_N six well-resolved frequencies appear, whereby two of the frequencies seem to be actually composed of two not resolvable components; i.e., the eight frequencies observed in zero field are also present in a nonzero external field. In effect the long-range antiferromagnetic or-

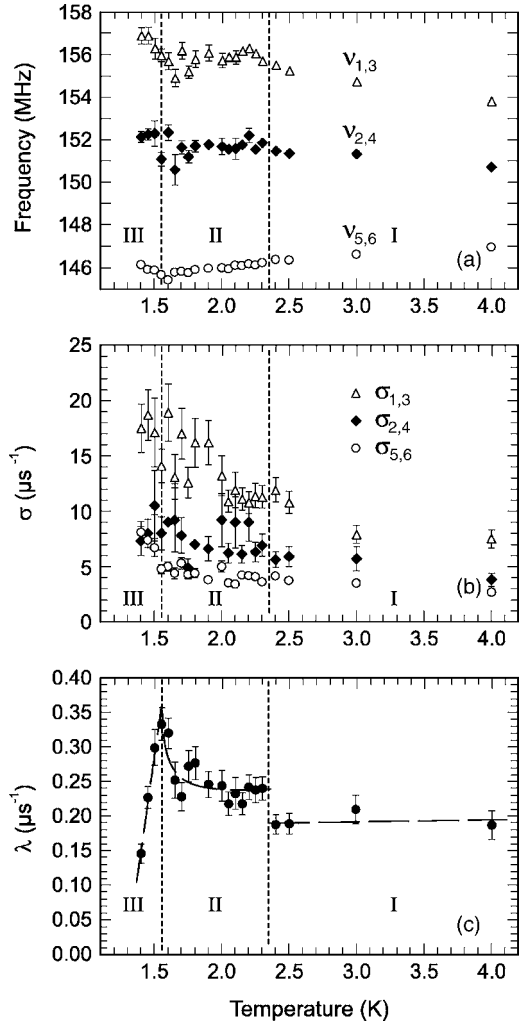

FIG. 11. Same as in Fig. 10, except that the data were taken at $B_{ext}=1.1$ T. Both the precession frequencies and the relaxation rates σ appear rather insensitive to the I-II and II-III phase transitions, in contrast to the behavior of the LF relaxation rates λ, panel (c).

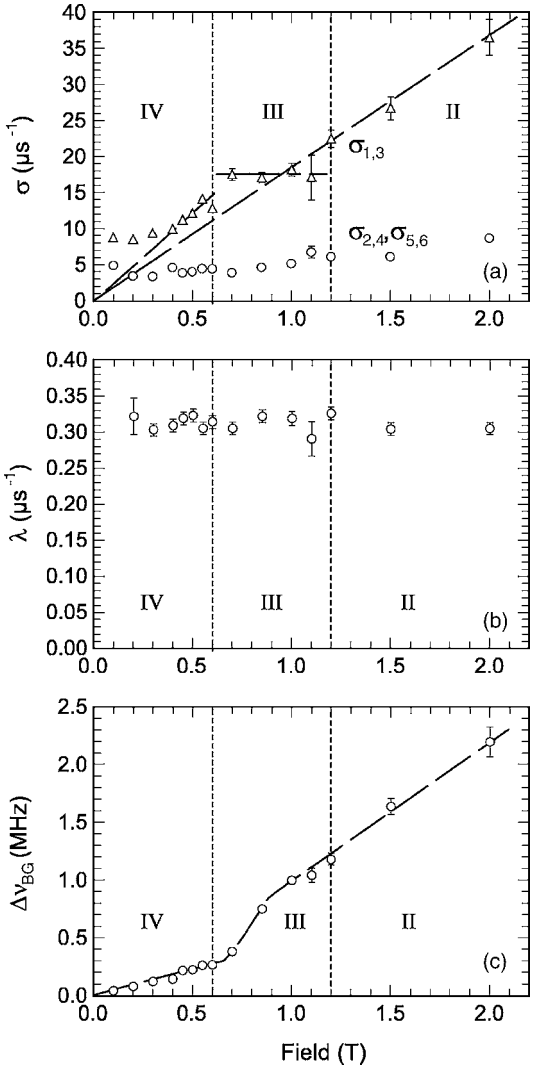

FIG. 12. Field dependence at 1.5 K of (a) the Gaussian TF relaxation rates $\sigma_{1,3}$ and $\sigma_{2,4}\simeq\sigma_{5,6}$, (b) the LF exponential relaxation rate λ, and (c) the width of the background signal arising from μ^+ stopped in the silver sample holder. The latter is proportional to the bulk susceptibility of the sample.

der in phase III of CeB_6 is well reflected in the μSR data. Figure 13 also shows that the temperature dependence of the two frequencies in phase I undergoes a drastic change when phase II is entered. None of that is seen in $Ce_{0.75}La_{0.25}B_6$, Figs. 10 and 11.

One may think of two explanations for the insensivity of the precession frequencies in $Ce_{0.75}La_{0.25}B_6$.

(i) The magnetic response and properties of the μ^+ nearest Ce neighbor(s) is strongly affected by the presence of the μ^+, so that, e.g., the nearest-neighbor (NN) Ce ions remain paramagnetic down to the lowest temperatures. This could also explain the absence of a further splitting when entering phase III. However, this hypothesis is contradicted by the fact that NN Ce ions in CeB_6 were seen *not* to be affected by the muon.[15,17] Also the ZF results imply that the NN Ce ions in both phase IV and phase III are involved in the magnetic order, since otherwise the magnitude of the ZF σ could not be understood. As to the σ_i values in transverse field, see below.

(ii) Since the Knight shift generally reflects the local magnetic response, in particular the atomic (Van Vleck) susceptibility of the nearest Ce neighbors, it is clear that in the present case the local magnetic response is insensitive to the different phases in contrast to CeB_6. The difference between the bulk magnetic response and the local magnetic response below 10 K must then be a contribution which does not lead to hyperfine fields at the μ^+, also not via some contact hyperfine mechanism. If this contribution is associated with the conduction electrons or electron states not centered on the Ce sites, it is possible that they are to be found at the La sites and are, in this sense, induced by the La doping.

The invisibility of the different phases and phase boundaries in the temperature dependence of the precession frequencies is even more evident, when examining the Knight shifts extracted from the frequencies $\nu_{1,3}$ and $\nu_{2,4}$, which are associated with the d sites with two Ce ions or one Ce and one La ion as nearest neighbors, respectively. In order to extract the Knight shift the Lorentz and demagnetization contributions to the ν_i had to be substracted first. Both con-

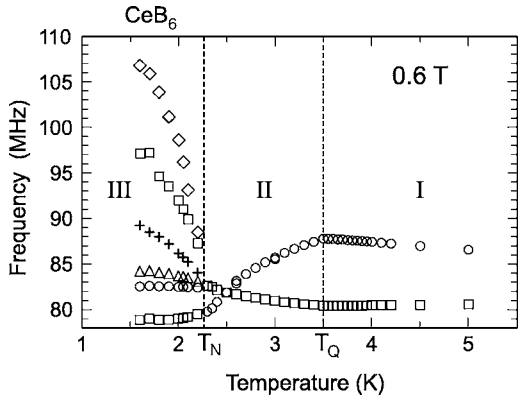

FIG. 13. Temperature dependence of the two precession frequencies observed in CeB_6 at B_{ext}=0.6 T above T_N and the splitting into at least six precession frequencies below $T_N \simeq 2.25$ K. Note also the change in behavior at T_Q, the transition from phase I (paramagnetic) to phase II (antiferroquadrupolar ordered). From Ref. 16 and unpublished data.

tributions are proportional to the magnetic susceptibility χ. The temperature dependence of χ at 0.3 T was taken from the literature;[27,47] the temperature dependence at 1.1 T and the field dependence of χ at 1.5 K were extracted from the relaxation of the background signal, as already indicated [see, e.g., Fig. 12(c)]. The results for K_1 (ex $\nu_{1,3}$) and K_2 (ex $\nu_{2,4}$) are displayed in Fig. 14. Obviously the Knight shifts are independent of the fields, K_2 remains half the value of K_1, and no traces of the various phase boundaries are visible. Also included in Fig. 14 is K_1 observed in CeB_6, where the clear visibility of the I-II phase transition is in striking contrast to the $Ce_{0.75}La_{0.25}B_6$ case. This raises the question about the identity of phases II in the two compounds.

At this point we recall that, in previous studies of $PrCu_2$ (Ref. 48) and CeAg (Ref. 49) both possessing a FQ-ordered phase, the μ^+ Knight shift showed also no anomaly or change at the transition to this FQ state. This was explained

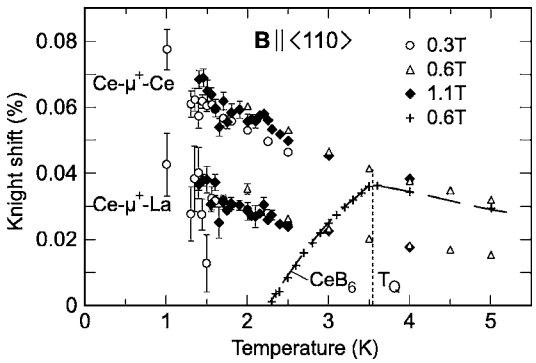

FIG. 14. Temperature dependence of the Knight shifts K_1 (ex $\nu_{1,3}$) and K_2 (ex $\nu_{2,4}$) collected at B_{ext}=0.3 T, 0.6 T, and 1.1 T. K_1 originates from μ^+ with two nearest-neighbor Ce atoms and K_2 from μ^+ with one La and one Ce atom as nearest neighbors. In both cases the μ^+ reside at the d sites $(\frac{1}{2}00)$ and $(0\frac{1}{2}0)$ with $\boldsymbol{B}_{ext} \| \langle 110 \rangle$. Also shown is the corresponding Knight shift observed in CeB_6. (Refs. 16 and 17). Note the insensitivity of K_1 and K_2 to the various phase transitions, in particular to the I-II transition at 1.1 T and ~2.3 K, in contrast to the behavior in CeB_6.

by the assumption that already in the normal (paraquadrupolar) phase a field induced FQ state (FIFQ) state exists, with no change when the ZF spontaneous FQ-ordered phase is established. The evidence for this FIFQ state was deduced from the unusual anisotropic contact hyperfine coupling constant. An anisotropic hyperfine coupling was also found in CeB_6 (Ref. 17) and in $Ce_{0.75}La_{0.25}B_6$ in the present work. Therefore we conjecture that phase II in $Ce_{0.75}La_{0.25}B_6$ could be a FQ-ordered phase, while phase II in CeB_6 is an anti-FQ state. This conjecture, however, is at odds with the absence of any significant softening of the elastic constants on going from phase I to phase II (Ref. 37) and the field dependence of $T_{I\text{-}II}$, which is the same as in CeB_6 and is explained to arise from a field-induced stabilization of the AFQ order as was mentioned in the introduction. In any case the strikingly different behavior of the μ^+ Knight shift across the I-II phase boundary in CeB_6 and $Ce_{0.75}La_{0.25}B_6$ indicates that phases II in the two compounds are not identical.

The behavior of the Knight shift is actually quite puzzling: since it should be proportional to the magnetic susceptibility and since the susceptibility is different in the different phases, one would have expected this to be reflected in the Knight shift, but this was not observed. Also, the temperature dependence of the susceptibility at the different fields is very different and neither reflected in the Knight shift. Rather it seems that the relevant local susceptibility, governing the Knight shift, is a smooth function of temperature, essentially field independent, and insensitive to the different phases.

In contrast, $\sigma_{1,3}$, $\sigma_{2,4}$, and $\sigma_{5,6}$ at 0.3 T do show strong variations—namely, qualitatively the same behavior as the Gaussian relaxation rate σ_{ZF} in zero field: a steep temperature dependence below $T_{I\text{-}IV}$ and, for $\sigma_{1,3}$ and $\sigma_{2,4}$, a change in slope at $T_{IV\text{-}III}$. No change in the slope seems to occur for $\sigma_{5,6}$. We also note that $\sigma_{1,3}$ is field independent in phase III [see Fig. 12(a)]. All this indicates clearly that at least $\sigma_{1,3}$ is not related to the field-induced and therefore susceptibility-dependent magnetism. Rather, the large $\sigma_{i,j}$ must originate from the spontaneous order in phase III, and phase IV as well. The average $\bar{\sigma}=(a_1\sigma_{1,3}+a_2\sigma_{2,4}+a_{5,6}\sigma_{5,6})/(a_1+a_2+a_{5,6})$ at 1 K and 0.3 T—i.e., in phase III—amounts to $\simeq 18.9\ \mu s^{-1}$. This value may be compared with the corresponding ZF σ: $\sigma_{ZF} \simeq 29\ \mu s^{-1}$. We find $\sigma_{ZF}/\bar{\sigma} \simeq 1.5 \simeq \sqrt{2}$. This is the expected ratio for a completely random and isotropic distribution for the microscopic internal fields.[50] Similarly, in phase IV at 1.5 K and 0.3 T we find $\bar{\sigma}_{ZF}/\bar{\sigma} \simeq 1.36 \simeq \sqrt{2}$. Therefore it seems that our previous conclusions are confirmed: namely, that the strong internal fields in both phase IV and phase III arise from some random or sufficiently short-range magnetic order.

However, this magnetic order cannot be completely random. Remembering that $\sigma_{1,3}$ originates from muons residing at d sites (1/2 0 0) and (0 1/2 0), while σ_5 from muons at sites (0 0 1/2), we can calculate the corresponding second moments M_2 for the spread of truely random fields. The result is $M_2^{(1/2\ 0\ 0)}=M_2^{(0\ 1/2\ 0)}=2.92\times 10^{16}\ \mathrm{MHz}^2/\mu_B^2=\sigma_{1,3}^2$ and $M_2^{(0\ 0\ 1/2)}=4.10\times 10^{16}\ \mathrm{MHz}^2/\mu_B^2=\sigma_5^2$, or $\sigma_5>\sigma_{1,3}$, also $\sigma_6>\sigma_{2,4}$. The measurement, however, shows the opposite. (Whether generally also $\sigma_{2,4}>\sigma_6$ cannot be determined, since the component ν_6 is masked by the stronger ν_5.) Hence,

a truely random order of the Ce^{3+} moments can be excluded. In the TF case the field spread $\Delta B = \sigma/\gamma_\mu$ relates only to the component along $\boldsymbol{B}_{\text{ext}}$, where the field is parallel to the $\langle 110 \rangle$ axis. In order to reproduce $\sigma_{1,3} > \sigma_5$ we would have to assume that the fields of the ordered moments are mostly perpendicular to $\boldsymbol{B}_{\text{ext}}$ at the site (0 0 1/2) and possess a strong component along the field for the two other sites. Considering dipolar fields, such a situation becomes possible if the ordered moments are more or less confined to the plane (0 0 1) containing the external field. In particular, the moments may be aligned along $\langle 110 \rangle$ in agreement with Refs. 9 and 32, while alignments along $\langle 101 \rangle$ or $\langle 011 \rangle$ have to be excluded. This would imply that in the presence of a nonzero external field a single-domain situation is established (an analogous situation in phase III of CeB_6 has been proposed in Ref. 39).

Note that $\sigma_{2,4}$ also originates from muons at the *d* sites (1/2 0 0) and (0 1/2 0), but one of the nearest neighbors is now replaced by nonmagnetic La; i.e., a source of internal field is missing, hence $\sigma_{2,4} \lesssim 0.5 \times \sigma_{1,3}$.

Since $\sigma_{1,3} > \sigma_{5,6}$ also in phase IV, the single-domain picture would apply here as well. Note that in phase IV (but not in phase III) one has $\sigma_{2,4} \approx \sigma_{5,6}$. This is reasonable, since empirically $\sigma_{5,6} \approx 0.5 \times \sigma_{1,3}$ and, as expected, $\sigma_{2,4} \approx 0.5 \times \sigma_{1,3}$. The small values of $\sigma_{2,4}$ in phase III may indicate a change of magnetic properties for a Ce ion next to a magnetic hole.

Turning to the 1.1-T data (Fig. 11) we see that in this case also the damping rates σ_i do not show any clear anomalies at $T_{III\text{-}II}$ and $T_{II\text{-}I}$. In contrast, the I-II phase transition in CeB_6 is reflected by a steep increase of the corresponding Gaussian relaxation rates, which are, however, roughly an order of magnitude smaller than in the present case.[51] The magnitudes of the σ_i are of the same order as at 0.3 T in phase III and therefore appear not to be field induced, as noted above, whereas in phase I the σ_i are significantly larger at 1.1 T than at 0.3 T. This is more clearly seen in the field scans performed at 1.5 K [see Fig. 12(a)]: σ_1 scales with B_{ext} in phase IV above 0.3 T up to the boundary to phase III and again in phase II, while σ_1 is essentially field independent in phase III. On the other hand, $\sigma_{2,4} \simeq \sigma_{5,6}$ displays a much weaker field dependence with no clear anomalies at the various phase boundaries. The field independence of $\sigma_{1,3}$ in phase III appears reasonable since the (antiferro)magnetic order is fully established and the external fields in the range covered in this experiments have no effect on the ordered moments. The field independence of σ_1 in phase IV below 0.3 T may testify to the emerging nature of the magnetic order in this phase. The perfect scaling of $\sigma_{1,3}$ in phase II is in accordance with the absence of any magnetic order.

It should be mentioned that $\sigma_{1,3}$, $\sigma_{2,4}$, and $\sigma_{5,6}$ scale with the bulk susceptibility χ_{bulk} above 8 K, while below 8 K the σ_i increase much faster than χ_{bulk} (data are not shown).

The present TF-μSR results may be compared with ^{11}B-NMR data[33,46] on $Ce_{0.75}La_{0.25}B_6$. In phase IV an appreciable NMR-line broadening, starting just below $T_{IV\text{-}I}$, is observed which looks very similar to our ZF and TF (0.3 T) results. Also below $B_{\text{ext}} = 0.48$ T the full width half maximum (FWHM) of the NMR signal shows little field dependence. The authors conclude that the magnetic properties in phase IV must be similar to the ones in phase III.[46] In phase III the NMR spectrum, using a single crystal, shows a broad unresolved but structured signal in contrast to well-split narrow signals obtained in phase III of CeB_6.[33] The broad signal could be fitted by a model which includes AFM and octupole magnetic order, suggesting that the AFM order is similar to the order in CeB_6.[32] However, the extracted dipolar order parameter does not vanish at $T_{III\text{-}IV}$, consistent with the conclusion that the magnetic order first develops in phase IV and becomes fully established in phase III.

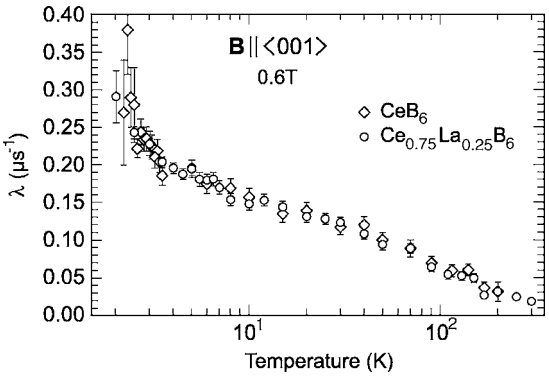

FIG. 15. Temperature dependence of the LF (0.6 T) exponential relaxation rate λ in phase I in CeB_6 and $Ce_{0.75}La_{0.25}B_6$. Note the perfect agreement.

Unfortunately, as far as we know, no NMR data are available in phase II, which is considered, like in CeB_6, to have no magnetic order in zero field, but may develop some (simple) AFM order in the presence of an external field. As noted above $\sigma_{1,3}$ and $\sigma_{2,4}$ appear unaffected by crossing the III-II-phase boundary; however, $\sigma_{5,6}$ increases below $T_{III\text{-}II}$ significantly, Fig. 11. If in phase III the same AFM order is estblished as in CeB_6, as implied by the neutron scattering work,[32] one would at least have expected that all σ_i were to rise dramatically in view of the strong increase of the splitting of the μSR frequency spectrum as seen in CeB_6. The absence of such behavior appears to rule out that in phase III at a field of 1.1 T the same type of long-range double-***k*** structure is formed as in CeB_6.

VI. LONGITUDINAL FIELD MEASUREMENTS IN PHASES I, II, III, AND IV

A. Experimental results

As mentioned in Sec. II, the LF data could be collected in parallel to the TF data. The spectra obtained in the forward and backward counters displayed a simple exponential depolarization ($B_{\text{ext}} \geqslant 0.2$ T)

$$aP(t) = a \exp(-\lambda t). \tag{16}$$

The fit results from the temperature scans at the fields 0.3 T and 1.1 T are collected in Figs. 10(c) and 11(c), respectively, and from the field scan at 1.5 K in Fig. 12(b). Figure 15 displays λ at higher temperatures (only phase I) both in CeB_6 and $Ce_{0.75}La_{0.25}B_6$ at 0.6 T from 2 K up to 300 K.

B. Discussion of the LF results

Figures 10(c) and 11(c) demonstrate that the various phase boundaries are clearly reflected in the spin lattice relaxation rate $\lambda(T)$, implying that the underlying spin dynamics changes significantly from phase to phase. The transition from phase I to phase IV at the field 0.3 T is characterized by a cusp like anomaly, typical for a magnetic phase transition of second order. The same was also seen in the ZF data, Fig. 8(c), and in the nuclear spin lattice relaxation $1/T_1$ at 0.48 T.[46] The transition from phase IV to phase III is marked by an accelerated decrease of $\lambda(T)$ with decreasing temperature. Note that, in ZF, $\lambda(T)$ did not show any clear anomaly at $T_{III\text{-}IV}$, Fig. 8(c). These data seem to confirm that the onset of the dipolar order is really at $T_{I\text{-}IV}$ and the transition at $T_{III\text{-}IV}$ only slightly modifies the magnetic state. At 1.1 T the transition from phase I to phase II is characterized by a steplike change of λ and by a cusplike anomaly at the transition to phase III. The latter is again consistent with a second-order magnetic phase transition, the former perhaps with a first-order transition. Data taken at 0.6 T for $T \geqslant 2$ K (phase I) agree essentially with the 0.3 T data. However, puzzling is the apparent temperature independence of λ at 1.1 T above $T_{I\text{-}II}$ up to 4 K.

Figure 12(b) displays an essentially field-independent λ at 1.5 K—i.e., no dependence on the position in the phase diagram. This is somewhat accidental, since at lower or somewhat higher temperatures this independence is not seen. However, above $\approx$4 K in phase I, λ becomes truly field independent. Nevertheless, Fig. 12(b) may be taken as evidence that the spin fluctuations are so fast that $\omega\tau_c \ll 1$, where ω is the μ^+ Larmor frequency and $1/\tau_c$ the fluctuation rate. Note that also the zero field λ at 0.1 K is the same at 0.3 T. In this fast fluctuation limit λ may be written as

$$\lambda = (\gamma_\mu A)^2 \tau_c, \tag{17}$$

where A is the fluctuating field amplitude. The decrease of λ in phases IV and III reflects then primarily the shrinking amplitude of the fluctuating fields at the μ^+, while τ_c may become temperature independent and remains small. This could point to a decreasing number of isolated fluctuating Ce^{3+} spins.

Going to higher temperatures at a field of 0.6 T, $\lambda(T)$ decreases smoothly with only a slight change in the T dependence near 30 K, Fig. 15. Interestingly these latter data agree perfectly with $\lambda(T)$ measured under the same conditions in CeB_6 above T_Q. This implies that the spin dynamics speeds up rather slowly with increasing temperature. (Note that μ^+ diffusion is not present up to at least 200 K.) Since the fluctuating fields at the μ^+ arise fom the Ce ions, it is very puzzling why λ does not reflect the presence of magnetic holes in $Ce_{0.75}La_{0.25}B_6$. Comparing Figs. 8(b) with 10(c) it is evident that in phase IV and to a lesser extend in phase III the applied field does modify the spin dynamics, either by decreasing the fluctuation rate or by increasing the fluctuating field amplitude [see Eq. (17)]—e.g., via affecting, in the ordered state, the spatial correlations of the fluctuating spin components. The equality of λ in ZF and in LF at 1 K points then to a rather rigid spin structure at low T, not influenced by $B_{ext} \leqslant 1.1$ T.

VII. SUMMARY AND CONCLUSIONS

The present μSR results unambiguously show that magnetism in phase III of $Ce_{0.75}La_{0.25}B_6$ is *substantially* different from the AFM structure of the parent CeB_6. Although earlier neutron diffraction[31,32] and NMR[33] studies suggested identical magnetic structures for the two cases, the disappearence of the eight distinct μSR spectrum lines, replaced here by a continuous spectrum indicating random or sufficiently short-range-ordered (SRO) fields, indicates that the long-range AFM order of CeB_6 is absent in this compound. This is further corroborated by the absence of any additional splitting of the TF-μSR signal in phase III. In fact we have no plausible explanation for the inconsistency of the neutron and μSR results to offer.

As to the "enigmatic" phase IV, where both theory and recent experimental evidence indicate the magnetic octupole moment of Ce^{3+} as primary order parameter, the information given by μSR is entirely based on observing the concomitant[25] *dipolar* magnetism. (This is because the short ranged octupole field of a Ce^{3+} ion is difficult to distinguish at the distance of an interstititial μ^+ site.) The results show that the dipolar magnetic structures of phase III and IV in $Ce_{0.75}La_{0.25}B_6$ are very similar, short-range ordered or glass like random also in phase IV. These ZF and TF results are consistent with earlier NMR[33] and μSR studies,[35] and also with the RXS data,[25] which suggest a mesoscopic dipolar SRO coexisting with the AFO order.

An unexpected observation in zero field is that, on entering phase IV through $T_{III\text{-}IV}$ and increasing the temperature, the volume of the crystal starts to separate into magnetic and nonmagnetic domains and, by reaching the phase boundary IV-I, the nonmagnetic fraction (i.e., that showing no dipolar magnetism) attains 100%. Moreover, in the presence of an external field $\geqslant$0.3 T a single-domain magnetic "order" appears to be induced.

The present data, unlike the RXS result,[25] show no evidence for persisting magnetic order across the phase boundary IV-I. The onset of magnetic order at $T_{I\text{-}IV}$ is seen as a conspicuous cusplike anomaly in the spin-lattice relaxation rate λ, in agreement with earlier NMR data.[33] As to the behavior of λ at the III-IV phase transition, it is in both zero field and in the applied field of 0.3 T consistent with the above conclusion on the similarity of the dipolar magnetism in phases III and IV; the magnetic structure in phase IV can apparently be viewed as a precursor to phase III.

At $T_{II\text{-}III}$, in a field of 1.1 T, again a cusplike anomaly in λ appears, characterizing this transition as a truly magnetic one. On the other hand, the unchanged TF Gaussian relaxation rate σ at $T_{II\text{-}III}$ in the temperature scan may indicate that phase II has acquired magnetic properties due to the applied field, as has been observed in CeB_6 with its field-induced AFM order.

Probably the most surprising feature of the present work is the insensivity of the Knight shift to the various phase

transitions, in particular its field independence and the complete lack of scaling with the bulk magnetic susceptibility in the different parts of the phase diagram below ≈10 K. With respect to the I-II transition, the strikingly different Knight shift data in CeB_6 and $Ce_{0.75}La_{0.25}B_6$ seem to rule out that the phases II in the two compounds are identical. However, as for the other transitions, one is forced to conclude that they do not affect the part of the magnetic susceptibility relevant for the μ^+ Knight shift.

More information could be gained by NMR measurements covering phase II and the adjoining transitions, such measurements are strongly called for.

ACKNOWLEDGMENTS

We sincerely thank S. Kunii, Tohoku University, Sendai, for providing the high quality $Ce_{0.75}La_{0.25}B_6$ single crystals, thus enabling the present work. We are indebted to Oksana Zaharko, PSI, for remeasuring some of the susceptibility data in phases I and II, in particular at 1.1 T. These data scale almost perfectly with the corresponding dephasing rate of the background signal. We wish to thank the Laboratory for Muon-Spin Spectroscopy (LMU), in particular A. Amato and C. Baines and the crew of the proton accelerator of the Paul Scherrer Institut (PSI), for providing excellent measuring conditions.

[1] F. J. Ohkawa, J. Phys. Soc. Jpn. **52**, 3897 (1983).
[2] B. Zierngiebel, B. Hillebrands, S. Blumenrueder, G. Guntherodt, M. Loewenhaupt, J. M. Carpenter, K. Winzer, and Z. Fisk, Phys. Rev. B **30**, 4052 (1984).
[3] R. Shiina, O. Sakai, H. Shiba, and P. Thalmeier, J. Phys. Soc. Jpn. **66**, 3005 (1997); **67**, 941 (1998).
[4] K. N. Lee and B. Bell, Phys. Rev. B **6**, 1032 (1972).
[5] D. Hall, Z. Fisk, and R. G. Goodrich, Phys. Rev. B **62**, 84 (2000).
[6] S. Nakamura, T. Got, S. Kunii, K. Iwashita, and A. Tamaki, J. Phys. Soc. Jpn. **63**, 623 (1994).
[7] R. G. Goodrich, D. P. Young, D. Hall, L. Balicas, Z. Fisk, N. Harrison, J. Betts, A. Migliori, F. M. Woodward, and J. W. Lynn, Phys. Rev. B **69**, 054415 (2004).
[8] J. M. Effantin, J. Rossat-Mignod, P. Burlet, H. Bartholin, S. Kunii, and T. Kasuya, J. Magn. Magn. Mater. **47–48**, 145 (1985).
[9] O. Zaharko, P. Fischer, A. Schenck, S. Kunii, P.-J. Brown, F. Tasset, and T. Hansen, Phys. Rev. B **68**, 214401 (2003).
[10] Y. Tanaka, U. Staub, Y. Narumi, K. Katsumata, V. Scagnioli, S. Shimomura, Y. Tabata, and Y. Onuki, Physica B **345**, 78 (2004).
[11] H. N. Kono, K. Kubo, and Y. Kuramoto, Physica B **359–361**, 971 (2005).
[12] M. Kawakami, J. Phys. Soc. Jpn. **50**, 432 (1981).
[13] M. Takigawa, J. Phys. Soc. Jpn. **52**, 728 (1983).
[14] S. V. Demishev, A. V. Semeno, Yu. Paderno, N. Yu. Shitsevalova, and N. E. Sluchanko, Phys. Status Solidi B **242**, R27 (2005).
[15] R. Feyerherm, A. Schenck, F. N. Gygax, Y. Onuki, and N. Sato, J. Magn. Magn. Mater. **140**, 1175 (1995).
[16] A. Schenck, F. N. Gygax, and S. Kunii, Phys. Rev. Lett. **89**, 037201 (2002).
[17] A. Schenck, F. N. Gygax, G. Solt, O. Zaharko, and S. Kunii, Phys. Rev. Lett. **93**, 257601 (2004).
[18] N. Sato, S. Kunii, I. Oguro, T. Komatsubara, and T. Kasuya, J. Phys. Soc. Jpn. **53**, 3967 (1984).
[19] H. Nakao, K. Magishi, Y. Wakabayashi, Y. Murakami, K. Koyama, K. Hiroto, Y. Endoh, and S. Kunii, J. Phys. Soc. Jpn. **70**, 1857 (2001).
[20] G. Uimin, Phys. Rev. B **55**, 8267 (1997).
[21] T. Furuno, N. Sato, S. Kunii, T. Kasuya, and W. Sasaki, J. Phys. Soc. Jpn. **54**, 1899 (1985).
[22] S. Kishimoto, A. Kondo, M. Kim, H. Tou, M. Sera, and F. Iga, J. Phys. Soc. Jpn. **74**, 2913 (2005).
[23] O. Sakai, R. Shiina, and H. Shiba, J. Phys. Soc. Jpn. **74**, 457 (2005).
[24] H. Kusunose and Y. Kuramoto, J. Phys. Soc. Jpn. **74**, 3139 (2005).
[25] D. Mannix, Y. Tanaka, D. Carbone, N. Bernhoeft, and S. Kunii, Phys. Rev. Lett. **95**, 117206 (2005).
[26] T. Tayama, T. Sakakibara, K. Tenya, H. Amitsuka, and S. Kunii, J. Phys. Soc. Jpn. **66**, 2268 (1997).
[27] T. Tayama, S. Honma, K. Tenya, H. Amitsuka, T. Sakakibara, and S. Kunii, Physica B **259**, 32 (1999).
[28] M. Hiroi, M. Sera, N. Kobayashi, and S. Kunii, Phys. Rev. B **55**, 8339 (1997).
[29] T. Morie, T. Sakakibara, T. Tayama, and S. Kunii, J. Phys. Soc. Jpn. **73**, 2381 (2004).
[30] S. Kobayashi, Y. Yoshino, S. Tsui, H. Tou, M. Sera, and F. Iga, J. Phys. Soc. Jpn. **72**, 2947 (2003).
[31] K. Iwasa, K. Kuwahara, K. Kohgi, P. Fischer, A. Donni, L. Keller, T. Hansen, S. Kunii, N. Metoki, Y. Koike, and K. Ohoyama, Physica B **329–333**, 582 (2003).
[32] P. Fischer, K. Iwasa, K. Kuwahara, M. Kohgi, T. Hansen, and S. Kunii, Phys. Rev. B **72**, 014414 (2005).
[33] K. Mizuno, K. Magishi, M. Kawakami, T. Saito, K. Koyama, and S. Kunii, Physica B **329–333**, 597 (2003).
[34] A. Schenck and G. Solt, J. Phys.: Condens. Matter **16**, S4639 (2004).
[35] H. Takagiwa, K. Ohishi, J. Akimitsu, W. Higemoto, R. Kadono, M. Sera, and S. Kunii, J. Phys. Soc. Jpn. **71**, 31 (2002).
[36] M. Akatsu, T. Goto, Y. Nemoto, O. Suzuki, S. Nakamura, and S. Kunii, J. Phys. Soc. Jpn. **72**, 205 (2003).
[37] O. Suzuki, S. Nakamura, M. Akatsu, Y. Nemoto, T. Goto, and S. Kunii, J. Phys. Soc. Jpn. **74**, 735 (2005).
[38] Y. Yoshino, S. Kobayashi, S. Tsuji, H. Tou, M. Sera, F. Iga, Y. Zenitani, and J. Akimitsu, J. Phys. Soc. Jpn. **73**, 29 (2004).
[39] H. Kusunose and Y. Kuramoto, J. Phys. Soc. Jpn. **70**, 1751 (2001).
[40] K. Kubo and Y. Kuramoto, J. Phys. Soc. Jpn. **73**, 216 (2004); **72**, 1859 (2003).
[41] T. Nagao and J. I. Igarashi, Phys. Rev. B **74**, 104404 (2006).
[42] See, e.g., *Muon Science*, edited by S. L. Lee, S. H. Kilcoyne, and R. Cywinski (SUSSP Publications, Edinburgh, and IOP Publishing, London 1999).
[43] A. Schenck, in *Muon Science* (Ref. 42), p. 39.
[44] The susceptibility per mole Ce is the same in CeB_6 and $Ce_{0.75}La_{0.25}B_6$ above 100 K and nearly the same below; see, e.g., Komatsubara *et al.*, J. Magn. Magn. Mater. **31–34**, 368 (1983).
[45] See, e.g., Y. J. Uemura, in *Muon Science* (Ref. 42), p. 85.

[46] K. Magishi, M. Kawabami, T. Saito, K. Koyama, K. Miyumo, and S. Kunii, Physica B **312–313**, 189 (2002).
[47] T. Takikawa, T. Sakakibara, K. Matsuhira, K. Tenya, H. Amitsuka, and S. Kunii, Physica B **281-282**, 561 (2000).
[48] A. Schenck, F. N. Gygax, and Y. Onuki, Phys. Rev. B **68**, 104422 (2003).
[49] A. Schenck, F. N. Gygax, D. Andreica, and Y. Onuki, J. Phys.: Condens. Matter **15**, 8599 (2003).
[50] A. Schenck, *Muon Spin Rotation Spectroscopy* (Adam Hilger, Bristol, 1965).
[51] A. Schenck and F. N. Gygax (unpublished).